Circulation
Cardiovascular Imaging
JOURNAL OF THE AMERICAN HEART ASSOCIATION

In vivo Detection of Vulnerable Atherosclerotic Plaque by MRI in a Rabbit Model

Alkystis Phinikaridou, Frederick L. Ruberg, Kevin J. Hallock, Ye Qiao, Ning Hua, Jason Viereck and James A. Hamilton

Circ Cardiovasc Imaging 2010;3;323-332; originally published online Mar 1, 2010;
DOI: 10.1161/CIRCIMAGING.109.918524
Circulation: Cardiovascular Imaging is published by the American Heart Association. 7272 Greenville Avenue, Dallas, TX 72514
 Print ISSN: 1941-9651. Online ISSN: 1942-0080

In vivo Detection of Vulnerable Atherosclerotic Plaque by MRI in a Rabbit Model

Alkystis Phinikaridou, PhD; Frederick L. Ruberg, MD; Kevin J. Hallock, PhD; Ye Qiao, PhD; Ning Hua, BSc; Jason Viereck, MD, PhD; James A. Hamilton, PhD

Background—The ability to identify atherosclerotic plaques with a high risk for sudden disruption before stroke or myocardial infarction would be of great utility. We used a rabbit model of controlled atherothrombosis to test whether in vivo MRI can noninvasively distinguish between plaques that disrupt after pharmacological triggering (vulnerable) and those that do not (stable).

Methods and Results—Atherosclerosis was induced in male New Zealand White (n=17) rabbits by cholesterol diet and endothelial denudation of the abdominal aorta. After baseline (pretrigger) MRI with and without gadolinium contrast, the rabbits underwent 2 pharmacological triggerings to induce atherothrombosis, followed by another MRI 48 hours later (post-triggering). Atherosclerosis was identified by the pretriggered images in all rabbits, and thrombosis was identified in 9 of 17 animals (53%) by post-trigger MRI. After the animals were euthanized, 95 plaques were analyzed; 28 (29.5%) had thrombi (vulnerable) and 67 did not (stable) (70.5%). Pretriggered MRI revealed comparable stenosis in stable and vulnerable plaques, but vulnerable plaques had a larger plaque area (4.8±1.6 versus 3.0±1.0 mm^2; $P=0.01$), vessel area (9.2±3.0 versus. 15.8±4.9 mm^2; $P=0.01$), and higher remodeling ratio (1.16±0.2 versus 0.93±0.2; $P=0.01$) compared with stable plaques. Furthermore, vulnerable plaques more frequently exhibited (1) positive remodeling (67.8% versus 22.3%; $P=0.01$), in which the plaque is hidden within the vessel wall instead of occluding the lumen; and (2) enhanced gadolinium uptake (78.6% versus 20.9%; $P=0.01$) associated with histological findings of neovascularization, inflammation, and tissue necrosis.

Conclusions—We demonstrate that in vivo MRI at 3.0 T detects features of vulnerable plaques in an animal model of controlled atherothrombosis. These findings suggest that MRI may be used as a noninvasive modality for localization of plaques that are prone to disruption. **(*Circ Cardiovasc Imaging*. 2010;3:323-332.)**

Key Words: MRI ■ atherosclerosis ■ thrombosis ■ gadolinium ■ remodeling

Acute coronary syndromes (ACS) such as unstable angina pectoris and myocardial infarction are the leading causes of death in the United States.[1] Histological studies demonstrate that ACS are usually triggered by rupture/erosion of vulnerable atherosclerotic plaques, which results in luminal thrombosis.[2,3] X-ray angiographic studies, which do not provide information about plaque composition, suggest that the majority of high-risk plaques cause <50% luminal narrowing.[4,5] In vivo MRI can estimate the degree of luminal narrowing and identify plaque components.[6–9] Contrast-enhanced MRI (CE-MRI) using gadolinium-diethylenetriamine penta-acetic acid (Gd-DTPA) has improved the discrimination between the fibrous cap and the lipid core[10,11] and necrotic core[12] and the visualization of coronary atherosclerosis.[13,14] Furthermore, dynamic CE-MRI has shown that uptake of Gd-DTPA is correlated with neovascularization[15,16] and inflammation,[17] both of which are increased in vulnerable plaques.

Clinical Perspective on p 332

The inability to study thrombotic events and plaque vulnerability before atherothrombosis in humans necessitates the use of animal models. The rabbit model of controlled atherothrombosis using an intermittent cholesterol diet followed by pharmacological triggering was introduced by Contantinides et al[18] and later modified by Abela et al.[19] Recently, we further modified the preparation/dietary protocol and demonstrated that such rabbits develop 6 of 8 types of plaques[20] classified by American Heart Association (AHA) criteria. Importantly, we[20] and others[19,21] have shown that pharmaco-

Received October 26, 2009; accepted February 22, 2010.

From the Department of Physiology and Biophysics (A.P., Y.Q., N.H., J.A.H.), the Department of Medicine (F.L.R.), Section of Cardiology, the Department of Radiology (F.L.R.), the Department of Anatomy and Neurobiology (K.J.H.), and the Department of Neurology (J.V.), Boston University School of Medicine, Boston, Mass; and the Department of Biomedical Engineering (J.A.H.), Boston University, Boston, Mass.

Guest Editor for this article was David A. Bluemke, MD, PhD.

The online-only Data Supplement is available at http://circimaging.ahajournals.org/cgi/content/full/CIRCIMAGING.109.918524./DC1.

Correspondence to Dr. James A. Hamilton, 700 Albany St, 3rd Floor, W-302, Department of Physiology and Biophysics, Boston University School of Medicine, Boston, MA 02118. E-mail jhamilt@bu.edu

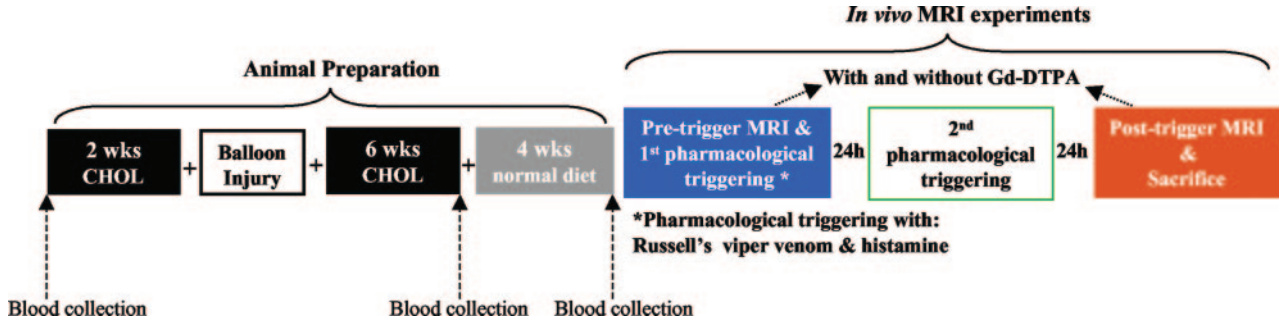

Figure 1. Experimental timeline. Rabbits were fed a 1% cholesterol diet for 2 weeks before and 6 weeks after balloon injury of the abdominal aorta, followed by 4 weeks of normal chow diet. In vivo MRI of the rabbit aorta is performed before (pretrigger) and after the second (post-trigger) pharmacological triggering. Plasma biomarkers were also monitored at baseline, after 8 weeks of cholesterol diet, and before triggering.

logically induced thrombosis occurs in plaques with histological features of vulnerability. In an alternative rabbit model of atherothrombosis, plaques were ruptured after an inflatable balloon was embedded into the plaque.[22] Although these rabbit plaques were histologically similar to human plaques, this model has not yet been used for MRI studies. In contrast, in vivo MR images of thrombosis associated with plaque disruption in the rabbit model of pharmacologically induced thrombosis have been reported.[23,24]

In this study, we used the rabbit model of experimentally induced atherothrombosis[20] to explore whether MR images obtained in vivo at 3.0 T could identify plaques prone to disruption.

Methods

Animal Model

Atherosclerosis was induced in adult male New Zealand White rabbits (n=24, ≈2.8 kg, Charles River Laboratories, Wilmington, Mass) as previously described.[20] Briefly, rabbits were fed a 1% cholesterol diet (PharmaServ, Framingham, Mass) for 2 weeks before and 6 weeks after balloon injury of the abdominal aorta, followed by 4 weeks of normal chow diet (Figure 1). Balloon injury of the aortic wall was performed under general anesthesia (acepromazine, 0.75 mg/kg IM; ketamine, 35 mg/kg IM; xylazine, 2.5 mg/kg IM). Pharmacological triggering of thrombosis was induced with Russell viper venom (0.15 mg/kg IP; Enzyme Research, South Bend, Ind) an activator of Factor X of the coagulation cascade followed 30 minutes later by histamine, a vasoconstrictor in rabbits (0.02 mg/kg IV; Sigma-Aldrich, St. Louis, Mo). This procedure was performed twice, within 48 hours, in each animal, as previously described.[18–21,23,24] Within 24 hours after the post-trigger MRI, the rabbits received heparin (1000 USP units IV, Sigma-Aldrich) to prevent postmortem blood clotting and were euthanized with a bolus injection of sodium pentobarbital (100 mg/kg IV). Subsequently, the aortas were excised and fixed in 10% formalin for histological analysis. Three age- and sex-matched, uninjured rabbits were fed only normal chow diet and used as controls.

Of the 7 rabbits that did not complete the study, 3 died prematurely from respiratory distress, ischemic heart disease, and/or liver failure (data not shown), 2 became anorexic early in the experimental protocol and were returned to normal diet, and 2 rabbits became paralyzed from the waist down after the first pharmacological triggering and were euthanized before the end of the protocol. Histological analysis of these 2 rabbits revealed occlusive thrombosis in the distal aorta (data not shown). Animal studies were performed in accordance with guidelines approved by the Institutional Animal Care and Use Committee of Boston University.

MRI Experiments

In vivo MRI experiments were performed on supine rabbits under deep sedation using a 3.0-T Philips Intera Scanner (Philips Medical Systems, Ohio) and a synergy knee coil with 6 elements. A pulse oximeter was placed on the ear for cardiac gating. The aorta of atherosclerotic rabbits was imaged before and 48 hours after the first pharmacological triggering (Figure 1). Control rabbits were imaged once. MRI acquisition parameters are listed in Table 1. Ungated coronal 3D phase contrast MR angiograms (PC-MRA) acquired with a T1-weighted, fast-filed echo sequence were used as scout images. Two-dimensional, T1-weighted, black-blood (T1BB) axial images (4 mm) were then acquired with a double-inversion recovery turbo-spin echo sequence and cardiac gating (at every other systolic phase). Subsequently, ungated axial 3D PC-MRA images were acquired immediately after a bolus injection of Gd-DTPA (0.1 mmol/kg IV) (Magnevist, Germany). For every axial T1BB slice (4 mm), 8 0.5-mm PC-MRA slices were acquired. Finally, post–contrast-enhanced (post-CE) T1BB images were acquired 10 to 15 minutes after Gd-DTPA injection with parameters identical to those used for the non–contrast-enhanced T1BB images.

Table 1. MRI Parameters

	3D Sagittal PC-MRA	Ungated 3D Axial PC-MRA	2D Axial T1BB
Slice thickness, mm	1	0.5	4
Interslice gap thickness, mm	0	0	1
TE, ms	3.5	7.4	10
Turbo factor	…	…	15
TR, ms	20	17	2 Cardiac cycles
Flip angle, degrees	15	15	90
Inversion recovery delay, ms	…	…	350
Black blood pulse thickness, mm	…	…	20
Flow velocity, cm/s	75	75	…
Field of view, mm (AP, FH, RL)	25×300×150	35×60×50	100×60×125
Matrix	256×244	128×122	384×362
Reconstructed resolution, mm	0.55×0.55×1	0.19×0.19×0.5	0.23×0.23
No. of averages	2	2	2
Scan time, min	3	8	8

Plasma Lipid and Inflammatory Marker Analysis

Blood samples were collected after overnight fasting from the ear artery at baseline, at the end of the 8-week cholesterol diet, and before triggering. Plasma total cholesterol and HDL-cholesterol (HDL-C) were measured with enzymatic reaction kits from BioVision (Mountain View, Calif) and Wako Chemicals Co (Richmond, Va), respectively. C-reactive protein and plasminogen activator inhibitor-1 were measured with ELISA kits from Immunology Consultant Laboratory (Newberg, Ore) and Molecular Innovations (Southfield, Mich), respectively.

Matching of MR Images and Histological Sections

The distances from the aortic renal branches and the iliac bifurcation were used as internal anatomic markers to match the MR images and histological sections.[20]

Histology and Identification of Vulnerable Plaques

Transverse cryosections (10 μm) were collected throughout the length of the each segment and stained with Masson trichrome (Sigma Aldrich) to identify cellular components and thrombi. Disrupted (vulnerable) plaques were defined as those with attached platelet and fibrin-rich thrombi. We have previously demonstrated that thrombosis in this model originates both from rupture of thin cap atheromas (60%) and superficial plaque erosion (40%), which frequently occurred over plaques classified by the AHA as atheromas and fibroatheromas and rarely over fibrotic plaques.[20] Plaques that had no overlying thrombus were defined as nondisrupted (stable).

Analysis of MR Images

Because the rabbits developed plaques throughout the region of the aorta that was balloon injured, we performed a slice-by-slice analysis of axial vessel wall images containing stable and vulnerable atherosclerotic plaques. Of the 204 pretriggered T1BB slices acquired from 17 rabbits, a total of 190 slices (95 before and 95 after gadolinium administration) and 1520 PC-MRA slices (760 anatomic and 760 flow-encoded) slices were evaluated. One hundred nine T1BB images were excluded from the analysis: 58 because either the T1BB or the PC-MRA slices were of poor image quality (insufficient blood suppression, bad signal-to-noise, motion artifacts) and 51 because the corresponding PC-MRA slices contained side branches that could impair the assessment of the remodeling ratio. Aortic regions containing plaques detected in the pretriggered MR images were classified into stable and vulnerable, based on the presence of luminal thrombosis seen on the post-triggered T1BB images and the corresponding histopathology. Subsequently, only the pretriggered MR images were analyzed using ImageJ (NIH).

Pre-CE T1BB images were used to calculate the plaque area (PA) and the percent cross-sectional narrowing (CSN) by manually segmenting the adventitial and luminal contours of the vessel wall. Plaque area was calculated as: PA=adventitial area−lumen area and the CSN as % CSN=(plaque area/vessel area)×100.

Ungated 3D PC-MRA images acquired immediately after injection of Gd-DTPA were used to calculate the remodeling ratio (RR) and the percent stenosis from flow-compensated/anatomic and flow-encoded images, respectively. In the anatomic images (T1-weighted spoiled-gradient echo) flowing blood appears bright, whereas the contrast of stationary tissues depends on the T1 relation times. In flow-encoded images, only flowing spins elicit signal, and the intensity is proportional to the velocity of flow, whereas stationary tissues are suppressed. It has been shown that spoiled-gradient echo images detect the adventitia/outer region of the vessel wall and that the delineation of this contour becomes improved in contrast-enhanced images.[25–27] A comparison of the vessel area measured on different MRI images is shown in Table 1 (supplemental data). Thus, at each lesion site, the anatomic images were used to measure the vessel area (VA) for the calculation of the RR, and the corresponding flow-encoded images were used to calculate the unobstructed lumen area (LA) and the percent stenosis. The RR and the percent stenosis were calculated after correcting for arterial tapering[28] and interindividual variability of arterial size.[29] The RR was calculated as $RR=\text{vessel area}_{lesion}/\text{vessel area}_{reference}$ (see Figure 3A) and the 3 remodeling categories were defined as previously described[30]: positive if RR >1.05, intermediate if $0.95 \leq RR \leq 1.05$, and negative if RR <0.95. The percent stenosis was calculated as $\%\ \text{stenosis}=1-[\text{lumen area}_{lesion}/\text{lumen area}_{reference}]\times 100$. Because of diffuse vessel wall thickening, the slice with the least amount of plaque was used as a reference site, assuming that it was least affected by the disease (mean values of references: PA=2.0±0.56 mm^2, VA=11.0±3.5 mm^2, LA=7.2±1.5 mm^2 and % CSN=21.4±6.3).

Post-CE T1BB images were visually compared with the pre-CE T1BB images to evaluate the presence or absence of a circumferential (full ring) or crescent-shaped enhancement pattern of the vessel wall. Bright signal from perivascular lymphatics and/or adipose tissue was sometimes visible in the pre-CE T1BB images. To eliminate ambiguities in the evaluation of the enhancement pattern of gadolinium-enhanced images, these regions were outlined on the pre-CE T1BB images and subsequently masked onto the gadolinium-enhanced images.

Statistical Analysis

Analyses were performed using SPSS 11.0 (SPSS Inc). For 2-group comparisons, continuous variables were compared using either a 2-sample t test or a Mann-Whitney nonparametric test after the variables were ranked. Categorical variables were compared using the χ^2 test. Qualitative data are presented as frequencies. Two independent observers (A.P. and J.V.) analyzed the pre-CE T1BB images to calculate the plaque area and evaluated the enhancement pattern on the post-CE T1BB images. In addition, 2 independent observers (A.P. and N.H) analyzed the PC-MRA images to calculate the vessel and lumen areas. Observers (J.V and N.H) were blinded to the MRI and histological findings. The interobserver variability was assessed by using the interclass correlation coefficient (ICC) for continuous variables and Cohen κ for categorical variables. Independent predictors of plaque vulnerability were identified by multilogistic regression analysis after the plaques were categorized as vulnerable and stable. Variables exhibiting statistical significance in the univariate regression (ie, plaque area, vessel area, remodeling index, presence of gadolinium hyperenhancement, and presence of positive and negative remodeling) were then used in the multilogistic regression model. Multiple linear regression analysis was used to evaluate the relationship between plasma biomarkers and plaque vulnerability. The sensitivity, specificity, positive and negative predictive values (PPV and NPV), and diagnostic accuracy of the MRI features alone or in combination were calculated. Data are presented as mean±standard deviation. Probability values of $P<0.05$ were considered significant.

Results

Atherosclerosis and Thrombosis Can Be Imaged by MRI

Aortic plaques were located in vivo using the pretriggered MR images, and the sites of luminal thrombosis were visualized on MR images acquired 48 hours after pharmacological triggering. The sites of plaques, plaque disruptions, and thrombosis were validated by the corresponding histological sections. Atherosclerosis was observed in all rabbits, and thrombosis occurred in 9 of 17 (53%) of them. No atherosclerosis was observed in control rabbits. A total of 95 wall segments containing plaques were included in this study, of which 28 (29.5%) showed luminal thrombi and 67 did not (70.5%).

Figure 2 shows representative MR images and histopathology of a plaque that did not disrupt (Figure 2A through 2C) and a plaque that disrupted after triggering (Figure 2D through 2F). The pretriggered image of the stable plaque (Figure 2A) demonstrates an eccentric plaque that did not

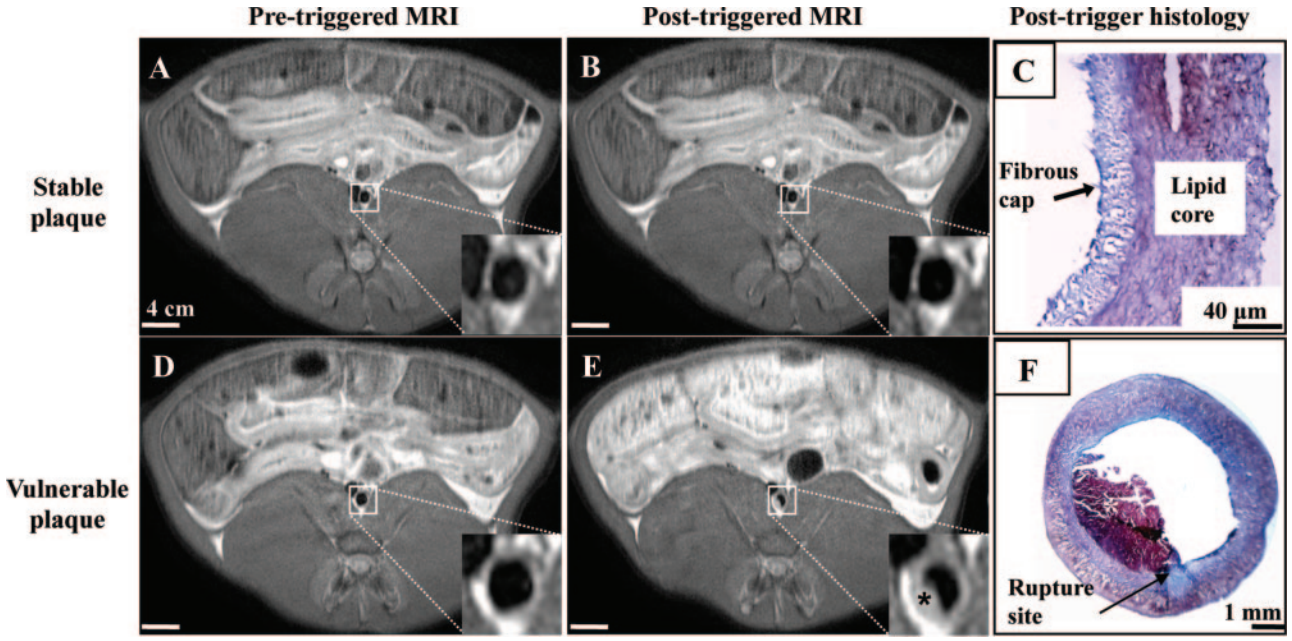

Figure 2. In vivo T1BB images and histopathology of stable and vulnerable plaques before and after pharmacological triggering (magnified views are provided at the bottom right of each pane). The stable plaque appeared similar on the pretrigger (A) and (B) post-trigger images. C, Corresponding histology showed a thick fibrous cap over a lipid core. D, Vulnerable plaque that formed a luminal thrombus after triggering (E; asterisk). F, Corresponding Masson trichrome staining revealed the site of rupture (arrow) and confirmed the presence of a platelet and fibrin-rich thrombus.

change in appearance after pharmacological triggering (Figure 2B). The corresponding histological section confirmed the presence of an intact fibrous cap overlaying a lipid-core (Figure 2C). The pretriggered image of the vulnerable plaque (Figure 2D) shows the plaque, whereas the post-triggered image shows a new mass protruding into the lumen (Figure 2E). The corresponding histology (Figure 2F) revealed the site of plaque rupture and confirmed the presence of an overlying platelet- and fibrin-rich thrombus.

Quantitative MRI and MRA Measurements of Stable and Vulnerable Plaques

Plaque area, vessel area, and remodeling ratio were significantly larger in vulnerable plaques; however, luminal area, percent stenosis, and percent CSN were similar between the 2 groups (Table 2). ICC revealed a high interobserver agreement for the measurements of vessel area (ICC, 0.92; 95% confidence interval [CI], 0.87 to 0.95) and luminal area (ICC, 0.9; 95% CI, 0.85 to 0.94) and moderate interobserver agreement for the measurement of plaque area (ICC, 0.64; 95% CI, 0.38 to 0.78).

Table 2. Quantitative MRI and MRA Measurements of Stable and Vulnerable Plaque

	Stable (n=67)	Vulnerable (n=28)	*P*
Plaque area, mm^2	3.0±1.0	4.8±1.6	0.01
Vessel area, mm^2	9.2±3.0	15.8±4.9	0.01
Lumen area, mm^2	7.0±1.4	7.5±1.2	0.19
% Stenosis	25.0±17.0	23.0±15.0	0.91
% Cross-sectional narrowing	39.3±14.3	34.9±11.0	0.16
Remodeling ratio	0.93±0.2	1.16±0.2	0.01

Vulnerable Plaques Are Associated With Positive Remodeling

A key finding from the analysis of the pretriggered images is that the plaques that disrupted after pharmacological triggering frequently exhibited positive remodeling (Figure 3). Pretriggered PC-MRA images acquired from the same rabbit demonstrate examples of negative and positive remodeling compared with a reference site. The vessel area measured at the site of the stable plaque (Figure 3B) was smaller than that of the reference site (Figure 3D), which is indicative of negative remodeling. In contrast, the vessel area of the vulnerable plaque (Figure 3F) was markedly larger than the reference site, suggestive of positive remodeling. Images of the lumen (Figure 3C, 3E, and 3G) demonstrate that this example of a stable plaque exhibited a greater extent of stenosis compared with that calculated for the vulnerable plaque. Overall, stable plaques frequently exhibited negative remodeling whereas vulnerable plaques frequently exhibited positive remodeling (Figure 3H). Similar findings were obtained when the frequency of the remodeling types in stable and vulnerable plaques was calculated using T1BB and post-CE T1BB images (Table 2; supplemental data).

Vulnerable Plaques Show Hyperintense Enhancement After Administration of Gd-DTPA

Another key finding that emerged from the analysis of the pretriggered MR images is the hyperintense signal associated with vulnerable plaques after administration of Gd-DTPA. A stable plaque that showed mild uptake of Gd-DTPA (Figure 4A and 4B) had a thick fibrous cap overlaying a lipid-core (Figure 4C). In contrast, vulnerable plaques demonstrated hyperintense circumferential (Figure 4E) or crescent-shaped enhancement (Figure 4H) that extended beyond the plaque. The

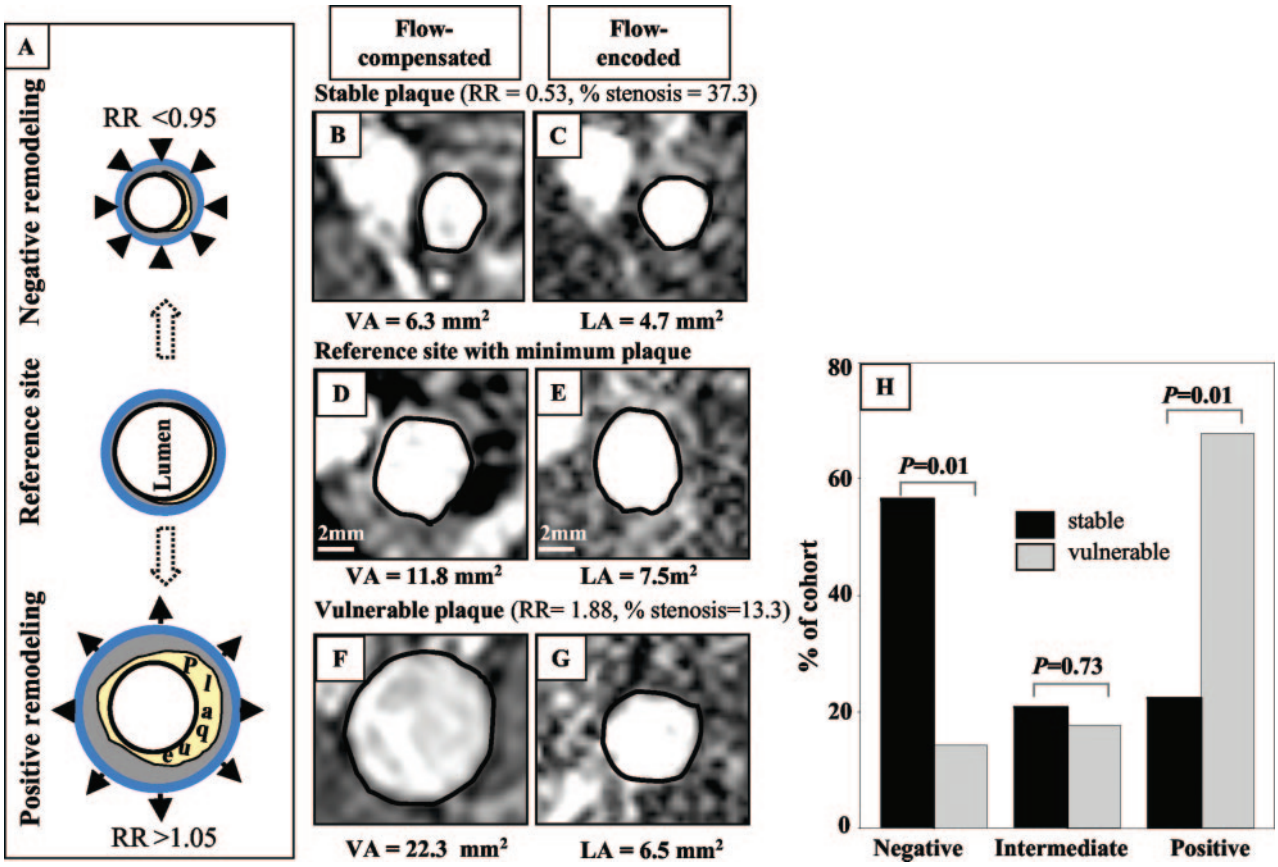

Figure 3. Examples of negative and positive remodeling in stable and vulnerable plaques. A, Types of vessel wall remodeling. The area circumscribed by the adventitial contour (blue line) indicates the vessel area. The remodeling ratio=vessel area$_{\text{lesion site}}$/vessel area$_{\text{reference}}$. The reference site is the site with the least amount of plaque. Positive remodeling and negative remodeling are defined from the remodeling ratio as shown. B to G, Examples of negative and positive remodeling in a stable (B to C) and a vulnerable (F to G) plaque compared with a reference site (D to E). B, D, and F, Flow-compensated images acquired with gadolinium showed negative remodeling at the site of a stable plaque (B) and positive remodeling at the site of a vulnerable plaque (H). C, E, and G, Flow-encoded images show the unobstructed luminal area. H, Frequency of negative, intermediate, and positive remodeling in stable and vulnerable plaques. Negative remodeling was significantly greater in stable plaques whereas positive remodeling was significantly greater in vulnerable plaques. Intermediate remodeling was similar between the 2 groups. RR indicates remodeling ratio; VA, vessel area; and LA, luminal area.

corresponding histology (Figure 4F and 4I) confirmed that a thrombus formed after pharmacological triggering and revealed extensive neovessels in the fibrous cap (Figure 4F; arrow), the intima, and the adventitia (Figure 4I; circles). Furthermore, histology revealed degradation of the extracellular matrix and tissue necrosis, 2 additional contributors of increased gadolinium uptake. Contrast enhancement of the vessel wall was not observed in control rabbits (data not shown).

The frequency of circumferential or crescent-shaped enhancement was statistically higher in vulnerable plaques whereas the absence of the hyperintense enhancement was statistically higher in stable plaques (Figure 4J). The Cohen κ statistic (κ=0.8) revealed a substantial interobserver agreement in evaluating the presence or absence of hyperintense enhancement after gadolinium administration.

The MRI features that discriminate stable and vulnerable plaques are shown in Table 3 and Figure 1 (Data Supplement). The presence of hyperenhancement on post-CE T1BB images showed the best sensitivity, specificity, PPV, NPV, and diagnostic accuracy. The NPV was high (97.6%), indicating accurate detection of stable plaque when the plaque was described by the presence of 1 of the 2 features (ie, positive remodeling or Gd-DTPA enhancement). The PPV was higher for plaques showing both features (positive remodeling and Gd-DTPA enhancement) than for plaques showing only 1 of these features, providing a high diagnostic accuracy (83.2%) for the detection of vulnerable plaque. The ability of positive remodeling, as calculated from 3 different types of MRI images, to identify vulnerable plaques is illustrated in Table 3 (supplemental data). The diagnostic accuracy was higher when the remodeling ratio was calculated using the CE-PCMRA. This suggests that CE-PCMRA images may improve the conspicuity of the outer vessel wall boundary and thereby provide a more accurate determination of the remodeling ratio.

Multilogistic regression analysis identified the gadolinium hyper-enhancement (P=0.01; odds ratio [OR], 13.46; 95% CI,3.17 to 57) and increased vessel area (P=0.004; OR, 1.36; 95% CI, 1.1 to 1.68) as independent predictors of plaque vulnerability. However, the regression model also showed that positive remodeling had values of P=0.11; OR, 4.7; 95% CI, 0.68 to 32.65; and negative remodeling, P=0.87; OR, 1.17; 95% CI, 0.15 to 9.13. These results, together with the fact that the higher diagnostic accuracy was achieved when

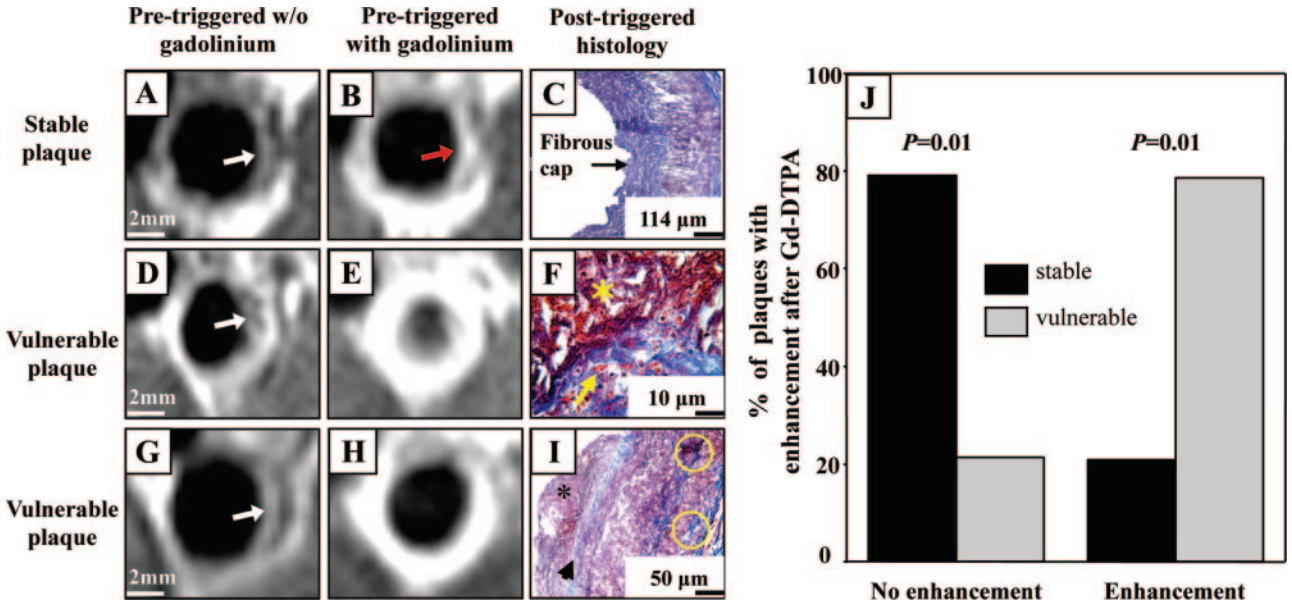

Figure 4. Uptake of gadolinium in stable and vulnerable plaques. Pretriggered T1BB MR images before (A, D, and G) and after (B, E, and H) injection of gadolinium-DTPA, with corresponding histological sections stained with Masson trichrome (C, F, and I). B, Stable plaque showed a mild enhancement (red arrow). C, Corresponding histology showed a thick fibrous cap overlaying a lipid core. E, Vulnerable plaque with circumferential enhancement. F, Histology verified that this was a vulnerable plaque that developed a thrombus after triggering. Red blood cell–filled neovessels (yellow arrow) spanned the fibrous cap underneath the thrombus. H, Vulnerable plaque with a crescent enhancement. I, Histology showed a luminal thrombus (asterisk) and a thin fibrous cap (arrowhead). Yellow circles indicate neovessels in the intima and adventitia. J, Frequency of the enhancement pattern after injection of gadolinium-DTPA in stable and vulnerable plaques. The frequency of the presence of circumferential and crescent-shaped enhancement pattern after injection of gadolinium was statistically higher in vulnerable compared with stable plaques.

both positive remodeling and gadolinium hyperenhancement were present, illustrate the value of multiple measurements to discriminate stable from vulnerable plaque.

Plasma Lipids and Inflammatory Markers Were Not Associated With Plaque Vulnerability

Measurement of plasma markers indicated the development of an atherogenic and inflammatory milieu under these experimental conditions (supplemental data; Table 4). Total cholesterol and C-reactive protein levels increased whereas plasminogen activator inhibitor-1 levels did not change significantly, in either group of rabbits. Importantly, HDL-C levels decreased after 8 weeks of cholesterol diet and returned to baseline after 4 weeks of normal diet. Despite these changes, there was no statistical difference in these biomarkers between rabbits with or without thrombi at any time point. In addition, multiple linear regression analysis revealed that none of these serum biomarkers was an independent predictor of thrombosis (supplemental data; Table 5).

Discussion

In this study, we used in vivo MRI to image the rabbit aorta before and after pharmacological triggering of thrombosis to discriminate vulnerable and stable plaques. After histological classification of the plaques into stable (70.5%) and vulnerable (29.5%) as determined by overlying thrombosis, we examined the MRI characteristics of the plaques in each category using the pretriggered images. To our knowledge, we demonstrate for the first time using in vivo MRI that vulnerable plaques are associated with (1) positive remodeling, in which the plaque remains hidden within the vessel wall instead of occluding the lumen; and (2) a circumferential or crescent-shaped hyperintense enhancement pattern after administration of Gd-DTPA, consistent with histological findings of neovascularization, inflammation, and tissue necrosis. The combination of both MRI findings provided a PPV of 87.5%, NPV of 82.3%, and diagnostic accuracy of 83.2%. Vulnerability was independent of the degree of stenosis and levels of plasma biomarkers. Regression analysis identified the hyperintense enhancement pattern on the post-CE images and increased vessel wall area as independent predictors of plaque vulnerability.

Several in vivo imaging methods, including MRI,[9–11,15–17,31] intravascular ultrasound (IVUS),[32–35] computed tomography,[36] and positron emission tomography,[37] have identified features associated with vulnerable plaques as determined by histological findings and/or clinical symptoms. However,

Table 3. MRI Features That Discriminate Stable and Vulnerable Plaque

	Sensitivity, %	Specificity, %	PPV, %	NPV, %	Diagnostic Accuracy, %
Positive remodeling	67.8	77.6	55.9	85.2	74.7
Gadolinium enhancement	78.5	79.1	61.1	89.8	78.9
Positive remodeling or gadolinium enhancement	96.4	59.7	50.0	97.6	70.5
Positive remodeling and gadolinium enhancement	50.0	97.0	87.5	82.3	83.2

these methods have not yet prospectively identified which plaques are likely to cause a cardiovascular event. Studies of human atherothrombosis are particularly challenging because plaque disruption cannot be controlled experimentally. The advantage of our rabbit model is that most types of human plaques can be replicated in the rabbit aorta and plaque disruption can be experimentally controlled.[20]

We found that positive remodeling was frequently associated with vulnerable plaques, whereas negative remodeling was frequently associated with stable plaques. As found for human vulnerable plaques in vivo,[4,5,32,38] the rabbit vulnerable plaques did not cause excessive luminal narrowing and were indistinguishable from stable plaques on the basis of luminal area or degree of stenosis, even though they had a larger plaque area than stable plaques. Positive remodeling has been recognized as a possible mechanism to alleviate luminal narrowing based on histological[39–41] and in vivo imaging studies.[34,35,42–44] However, only recently the association of positive remodeling with plaque vulnerability has been demonstrated in vivo by IVUS[32,33] and computed tomography.[36] In previous in vivo MRI studies of patients with subclinical coronary atherosclerosis[43,44] and of Watanabe hypercholesterolemic rabbits,[45] positive remodeling was observed as an increase in the vessel area, determined by the outer vessel wall contour, with concurrent preservation of the lumen area. Although these studies demonstrated that MRI can detect positive arterial remodeling in the presence of atherosclerosis, they did not quantify remodeling to provide a basis for comparison across subjects. On the other hand, IVUS studies have established standardized cut-off values for the classification of arterial remodeling.[30,32] Here, we demonstrated for the first time a noninvasive MRI method for classifying arterial remodeling using the cut-off values established by IVUS. We have previously demonstrated that positive remodeling was histologically associated with increased lipid content, inflammation, and medial and adventitial degradation in rabbit vulnerable plaques.[20] Furthermore, histological studies of human coronary arteries have suggested that positive remodeling and plaque vulnerability are linked through increased macrophage content[46] and secretion of matrix metalloproteinases,[47] which degrade the extracellular matrix promoting plaque instability. In contrast, although negative remodeling causes more luminal narrowing, it is associated with human stable plaques.[28]

In our study, the plaque burden assessed by calculating the percent CSN was similar between stable and vulnerable plaques. Studies of carotid atherosclerosis have shown that normalized wall index, which is similar to the percent CSN, correlated with complicated carotid plaques, intraplaque hemorrhage (IPH), and plaque rupture.[48] Conversely, another study[9] showed that the degree of atherosclerotic burden was similar between symptomatic and asymptomatic carotid plaques in subjects with unilateral atherosclerotic disease. We believe that these discrepancies might originate from the role of IPH in the natural progression of atherosclerotic disease. The presence of IPH accelerates plaque burden progression and increases the size of the lipid-rich necrotic core in asymptomatic subjects.[49,50] Furthermore, the later study[50] postulated that the rapid increase of plaque burden in the presence of IPH might occur because the local plaque environment changes too quickly to allow sufficient remodeling of the vessel wall to compensate for the sudden increase of plaque burden. However, in our rabbit model, IPH does not occur, which could account for the similar plaque burden found between stable and vulnerable plaque.

We also demonstrated that vulnerable rabbit plaques were associated with increased uptake of Gd-DTPA. Although all plaques showed some enhancement, the majority of vulnerable plaques had either a circumferential or crescent shape hyperenhancement pattern within the plaque and the surrounding vessel wall. Together with the presence of positive remodeling, this observation demonstrates that plaque vulnerability is more than a localized accumulation of lipids and thinning of the fibrous cap, 2 widely accepted histological features of plaque vulnerability. Aoki et al[51] were the first to observe a band of enhancement corresponding to the outer wall, which was attributed to angiogenesis of the wall itself. Enhancement of the outer rim was minimal in early phases of the disease and gradually increased. Studies of gadolinium-enhancement of the carotids reported excellent contrast between the fibrous cap and the lipid-core at 5 to 10 minutes after contrast agent administration[10] and that the uptake of gadolinium plateaus after the first 10 minutes.[52] In our study, we did not intend to use gadolinium to discriminate between plaque components. Our goal was to acquire delayed gadolinium-enhanced images at the plateau-phase and assess the overall uptake of the contrast agent. For this reason, a time interval of 10 to 15 minutes was chosen.

We have previously reported[20] that rabbit vulnerable plaques are characterized by increased histological changes including neovascularization, inflammation, tissue necrosis, and vessel wall disorganization. Therefore, we can attribute the increased uptake of Gd-DTPA reported herein to the presence of these histological changes. Our data are in agreement with previous studies that have demonstrated a correlation between gadolinium uptake and plaque neovascularization, inflammation, endothelial permeability, and fibrosis, both in human[12,13,15–17,53] and animal models.[16,54] Although we did not decipher the mechanisms that could account for the circumferential versus the crescent-shaped enhancement patterns, we postulate that circumferential enhancement involved a higher extent of the histological changes described above compared with the crescent-shaped enhancement. Furthermore, we found that stable plaques showed mild enhancement, whereas no enhancement of the aortic wall was observed in control rabbits. Our findings are consistent with previous studies that showed progressive uptake of Gd-DTPA with increasing severity of atherosclerosis both in patients with coronary artery disease[14] and hypercholesterolemic Watanabe rabbits[45] compared with no uptake in healthy subjects and minor uptake in control rabbits.

Although positive remodeling and gadolinium uptake were associated with vulnerable plaques both measurements showed false-positive and false-negative results. However, it is unlikely that clinical practice will change with 1 test for vulnerable plaque, with MRI or any other imaging modality. Rather, a combination of tests should be used to provide

greater confidence when choosing and/or monitoring therapy. For example, we demonstrated that combining positive remodeling and gadolinium enhancement provided a higher diagnostic accuracy (83.2%) for the detection of vulnerable plaque than either test alone (74% to 79%).

Study Limitations

One limitation of this rabbit model is the absence of plaque calcification and intraplaque hemorrhage. Although both features have been previously reported when rabbits were fed a similar cholesterol diet for much longer periods (8.5 months to 2 years) than those used in this study, animal mortality was increased because of generalized lipid toxicity.[21]

Another important issue is whether pharmacologically triggered plaque disruption in rabbits reflects spontaneous plaque rupture in humans. Although we[20] and others[19–21] have shown that pharmacologically induced thrombosis is associated with rabbit plaques that encompass histological features of plaque vulnerability, this methodology is a physiological approximation. Precisely what triggers human plaques to rupture or erode is unknown. Studies of canine[55] and human[56,57] coronary arteries have suggested that it involves platelet activation and adhesion and the release of vasoconstriction molecules, including thromboxane A2 and serotonin. Therefore, the combination of a procoagulant factor (viper venom) and a vasoconstriction agent (histamine) may be an acceptable physiological approximation. Furthermore, our accelerated model of atherosclerosis could result in a greater extent of atherosclerosis and a higher percentage of plaque disruption that one would expect in the natural history of atherothrombosis in humans. To this end, the higher percentage of disrupted plaques may alter the positive and negative predictive values of the MRI tests reported herein.

Another limitation of this study is that approximately one fourth of the MR images were excluded from the analysis due to poor image quality. In our current studies, improved pulse sequences, coil design, and animal positioning during scanning are being utilized. Finally, the contrast-enhanced images were acquired only at 10 to 15 minutes after administration of Gd-DTPA without the use of dynamic CE-MRI protocols that provide quantitative measurements of changes in signal intensity. We are currently exploring dynamic CE-MRI to quantify the temporal uptake of Gd-DTPA to (1) optimize the minimum dosage of gadolinium, (2) optimize the delay time between administration of gadolinium and image acquisition, (3) provide a quantitative comparison between stable and vulnerable plaque, and (4) provide a mechanism associated with gadolinium uptake.

Conclusions

Using a rabbit model of controlled atherothrombosis, we demonstrated that in vivo MRI can detect positive remodeling and increased uptake of Gd-DTPA, both of which were associated with vulnerable plaque and provided a high diagnostic accuracy for the discrimination of stable from vulnerable plaque. In contrast, thrombosis was independent of the degree of stenosis and levels of plasma biomarkers. The protocols reported in this study are promising because they are noninvasive, used the use of a clinically approved contrast agent, and were performed using a clinical MRI scanner.

Acknowledgments

We thank Drs Alexandros Tzatsos and Stephan Anderson for helpful comments during the preparation of the manuscript and Dr Michael LaValley for assistance with the statistical analysis.

Sources of Funding

This project was supported by NIH grant 5P50HL083801 (to Dr Hamilton).

Disclosures

Dr Hamilton has equity in a company (MRVimage) that could commercialize the technology. Boston University has filed a patent application on technology related to the article.

References

1. Lloyd-Jones D, Adams R, Carnethon M, De Simone G, Ferguson TB, Flegal K, Ford E, Furie K, Go A, Greenlund K, Haase N, Hailpern S, Ho M, Howard V, Kissela B, Kittner S, Lackland D, Lisabeth L, Marelli A, McDermott M, Meigs J, Mozaffarian D, Nichol G, O'Donnell C, Roger V, Rosamond W, Sacco R, Sorlie P, Stafford R, Steinberger J, Thom T, Wasserthiel-Smoller S, Wong N, Wylie-Rosett J, Hong Y. Heart disease and stroke statistics: 2009 update: a report from the American Heart Association Statistics Committee and Stroke Statistics Subcommittee. *Circulation*. 2009;119:480–486.
2. van der Wal AC, Becker AE, van der Loos C, Das P. Site of intimal rupture or erosion of thrombosed coronary atherosclerotic plaques is characterized by an inflammatory process irrespective of the dominant plaque morphology. *Circulation*. 1994;89:36–44.
3. Farb A, Burke AP, Tang AL, Liang TY, Mannan P, Smialek J, Virmani R. Coronary plaque erosion without rupture into a lipid core: a frequent cause of coronary thrombosis in sudden coronary death. *Circulation*. 1996;93:1354–1363.
4. Ambrose JA, Tannenbaum MA, Alexopoulos D, Hjemdahl-Monsen CE, Leavy J, Weiss M, Borrico S, Gorlin R, Fuster V. Angiographic progression of coronary artery disease and the development of myocardial infarction. *J Am Coll Cardiol*. 1988;12:56–62.
5. Giroud D, Li JM, Urban P, Meier B, Rutishauer W. Relation of the site of acute myocardial infarction to the most severe coronary arterial stenosis at prior angiography. *Am J Cardiol*. 1992;69:729–732.
6. Yuan C, Mitsumori LM, Ferguson MS, Polissar NL, Echelard D, Ortiz G, Small R, Davies JW, Kerwin WS, Hatsukami TS. In vivo accuracy of multispectral magnetic resonance imaging for identifying lipid-rich necrotic cores and intraplaque hemorrhage in advanced human carotid plaques. *Circulation*. 2001;104:2051–2056.
7. Cai JM, Hatsukami TS, Ferguson MS, Small R, Polissar NL, Yuan C. Classification of human carotid atherosclerotic lesions with in vivo multicontrast magnetic resonance imaging. *Circulation*. 2002;106:1368–1373.
8. Helft G, Worthley SG, Fuster V, Fayad ZA, Zaman AG, Corti R, Fallon JT, Badimon JJ. Progression and regression of atherosclerotic lesions: monitoring with serial noninvasive magnetic resonance imaging. *Circulation*. 2002;105:993–998.
9. Saam T, Cai J, Ma L, Cai YQ, Ferguson MS, Polissar NL, Hatsukami TS, Yuan C. Comparison of symptomatic and asymptomatic atherosclerotic carotid plaque features with in vivo MR imaging. *Radiology*. 2006;240:464–472.
10. Wasserman BA, Smith WI, Trout HH III, Cannon RO III, Balaban RS, Arai AE. Carotid artery atherosclerosis: in vivo morphologic characterization with gadolinium-enhanced double-oblique MR imaging initial results. *Radiology*. 2002;223:566–573.
11. Kramer CM, Cerilli LA, Hagspiel K, DiMaria JM, Epstein FH, Kern JA. Magnetic resonance imaging identifies the fibrous cap in atherosclerotic abdominal aortic aneurysm. *Circulation*. 2004;109:1016–1021.
12. Yuan C, Kerwin WS, Ferguson MS, Polissar N, Zhang S, Cai J, Hatsukami TS. Contrast-enhanced high resolution MRI for atherosclerotic carotid artery tissue characterization. *J Magn Reson Imaging*. 2002;15:62–67.
13. Maintz D, Ozgun M, Hoffmeier A, Fischbach R, Kim WY, Stuber M, Manning WJ, Heindel W, Botnar RM. Selective coronary artery plaque

visualization and differentiation by contrast-enhanced inversion prepared MRI. *Eur Heart J*. 2006;27:1732–1736.
14. Yeon SB, Sabir A, Clouse M, Martinezclark PO, Peters DC, Hauser TH, Gibson CM, Nezafat R, Maintz D, Manning WJ, Botnar RM. Delayed-enhancement cardiovascular magnetic resonance coronary artery wall imaging: comparison with multislice computed tomography and quantitative coronary angiography. *J Am Coll Cardiol*. 2007;50:441–447.
15. Kerwin W, Hooker A, Spilker M, Vicini P, Ferguson M, Hatsukami T, Yuan C. Quantitative magnetic resonance imaging analysis of neovasculature volume in carotid atherosclerotic plaque. *Circulation*. 2003;107:851–856.
16. Lin W, Abendschein DR, Haacke EM. Contrast-enhanced magnetic resonance angiography of carotid arterial wall in pigs. *J Magn Reson Imaging*. 1997;7:183–190.
17. Kerwin WS, O'Brien KD, Ferguson MS, Polissar N, Hatsukami TS, Yuan C. Inflammation in carotid atherosclerotic plaque: a dynamic contrast-enhanced MR imaging study. *Radiology*. 2006;241:459–468.
18. Constantinides P, Chakravarti RN. Rabbit arterial thrombosis production by systemic procedures. *Arch Pathol*. 1961;72:197–208.
19. Abela GS, Picon PD, Friedl SE, Gebara OC, Miyamoto A, Federman M, Tofler GH, Muller JE. Triggering of plaque disruption and arterial thrombosis in an atherosclerotic rabbit model. *Circulation*. 1995;91:776–784.
20. Phinikaridou A, Hallock KJ, Qiao Y, Hamilton JA. A robust rabbit model of human atherosclerosis and atherothrombosis. *J Lipid Res*. 2009;50:787–797.
21. Constantinides P. *Experimental Atherosclerosis.* New York, NY: Elsevier Publishing Co; 1965.
22. Rekhter MD, Hicks GW, Brammer DW, Work CW, Kim JS, Gordon D, Keiser JA, Ryan MJ. Animal model that mimics atherosclerotic plaque rupture. *Circ Res*. 1998;83:705–713.
23. Johnstone MT, Botnar RM, Perez AS, Stewart R, Quist WC, Hamilton JA, Manning WJ. In vivo magnetic resonance imaging of experimental thrombosis in a rabbit model. *Arterioscler Thromb Vasc Biol*. 2001;21:1556–1560.
24. Botnar RM, Perez AS, Witte S, Wiethoff AJ, Laredo J, Hamilton J, Quist W, Parsons EC Jr, Vaidya A, Kolodziej A, Barrett JA, Graham PB, Weisskoff RM, Manning WJ, Johnstone MT. In vivo molecular imaging of acute and subacute thrombosis using a fibrin-binding magnetic resonance imaging contrast agent. *Circulation*. 2004;109:2023–2029.
25. Kelekis NL, Semelka RC, Worawattanakul S, Molina PL, Mauro MA. Magnetic resonance imaging of the abdominal aorta and iliac vessels using combined 3-D gadolinium-enhanced MRA and gadolinium-enhanced fat-suppressed spoiled gradient echo sequences. *Magn Reson Imaging*. 1999;17:641–651.
26. Markl M, Dudler P, Fydrychowicz A, Strecker C, Weiller C, Hennig J, Harloff A. Optimized 3D bright blood MRI of aortic plaque at 3 T. *Magn Reson Imaging*. 2008;26:330–336.
27. Kerwin WS, Cai J, Yuan C. Noise and motion correction in dynamic contrast-enhanced MRI for analysis of atherosclerotic lesions. *Magn Reson Med*. 2002;47:1211–1217.
28. Pasterkamp G, Schoneveld AH, van Wolferen W, Hillen B, Clarijs RJ, Haudenschild CC, Borst C. The impact of atherosclerotic arterial remodeling on percentage of luminal stenosis varies widely within the arterial system: a postmortem study. *Arterioscler Thromb Vasc Biol*. 1997;17:3057–3063.
29. Shiomi M, Ito T, Hasegawa M, Yoshida K, Gould KL. Novel insights into coronary lumen preservation during progression of coronary atherosclerosis in coronary atherosclerosis-prone rabbits. *Coron Artery Dis*. 2004;15:419–426.
30. Pasterkamp G, Borst C, Gussenhoven EJ, Mali WP, Post MJ, The SH, Reekers JA, van den Berg FG. Remodeling of De Novo atherosclerotic lesions in femoral arteries: impact on mechanism of balloon angioplasty. *J Am Coll Cardiol*. 1995;26:422–428.
31. Choudhury RP, Fuster V, Fayad ZA. Molecular, cellular and functional imaging of atherothrombosis. *Nat Rev Drug Discov*. 2004;3:913–925.
32. Schoenhagen P, Ziada KM, Kapadia SR, Crowe TD, Nissen SE, Tuzcu EM. Extent and direction of arterial remodeling in stable versus unstable coronary syndromes : an intravascular ultrasound study. *Circulation*. 2000;101:598–603.
33. von Birgelen C, Klinkhart W, Mintz GS, Papatheodorou A, Herrmann J, Baumgart D, Haude M, Wieneke H, Ge J, Erbel R. Plaque distribution and vascular remodeling of ruptured and nonruptured coronary plaques in the same vessel: an intravascular ultrasound study in vivo. *J Am Coll Cardiol*. 2001;37:1864–1870.
34. Losordo DW, Rosenfield K, Kaufman J, Pieczek A, Isner JM. Focal compensatory enlargement of human arteries in response to progressive atherosclerosis: in vivo documentation using intravascular ultrasound. *Circulation*. 1994;89:2570–2577.
35. Nishioka T, Luo H, Eigler NL, Berglund H, Kim CJ, Siegel RJ. Contribution of inadequate compensatory enlargement to development of human coronary artery stenosis: an in vivo intravascular ultrasound study. *J Am Coll Cardiol*. 1996;27:1571–1576.
36. Motoyama S, Kondo T, Sarai M, Sugiura A, Harigaya H, Sato T, Inoue K, Okumura M, Ishii J, Anno H, Virmani R, Ozaki Y, Hishida H, Narula J. Multislice computed tomographic characteristics of coronary lesions in acute coronary syndromes. *J Am Coll Cardiol*. 2007;50:319–326.
37. Rudd JHF, Warburton EA, Fryer TD, Jones HA, Clark JC, Antoun N, Johnstrom P, Davenport AP, Kirkpatrick PJ, Arch BN, Pickard JD, Weissberg PL. Imaging atherosclerotic plaque inflammation with [18F]-fluorodeoxyglucose positron emission tomography. *Circulation*. 2002;105:2708–2711.
38. Smits PC, Pasterkamp G, de Jaegere PP, de Feyter PJ, Borst C. Angioscopic complex lesions are predominantly compensatory enlarged: an angioscopy and intracoronary ultrasound study. *Cardiovasc Res*. 1999;41:458–464.
39. Crawford T, Levene CI. Medial thinning in atheroma. *J Pathol Bacteriol*. 1953;66:19–23.
40. Bond MG, Adams MR, Bullock BC. Complicating factors in evaluating coronary artery atherosclerosis. *Artery*. 1981;9:21–29.
41. Glagov S, Weisenberg E, Zarins CK, Stankunavicius R, Kolettis GJ. Compensatory enlargement of human atherosclerotic coronary arteries. *N Engl J Med*. 1987;316:1371–1375.
42. McPherson DD, Sirna SJ, Hiratzka LF, Thorpe L, Armstrong ML, Marcus ML, Kerber RE. Coronary arterial remodeling studied by high-frequency epicardial echocardiography: an early compensatory mechanism in patients with obstructive coronary atherosclerosis. *J Am Coll Cardiol*. 1991;17:79–86.
43. Kim WY, Stuber M, Bornert P, Kissinger KV, Manning WJ, Botnar RM. Three-dimensional black-blood cardiac magnetic resonance coronary vessel wall imaging detects positive arterial remodeling in patients with nonsignificant coronary artery disease. *Circulation*. 2002;106:296–299.
44. Miao C, Chen S, Macedo R, Lai S, Liu K, Li D, Wasserman BA, Vogel-Claussen J, Lima JA, Bluemke DA. Positive remodeling of the coronary arteries detected by magnetic resonance imaging in an asymptomatic population: MESA (Multi-Ethnic Study of Atherosclerosis). *J Am Coll Cardiol*. 2009;53:1708–1715.
45. Steen H, Lima JA, Chatterjee S, Kolmakova A, Gao F, Rodriguez ER, Stuber M. High-resolution three-dimensional aortic magnetic resonance angiography and quantitative vessel wall characterization of different atherosclerotic stages in a rabbit model. *Invest Radiol*. 2007;42:614–621.
46. Varnava AM, Mills PG, Davies MJ. Relationship between coronary artery remodeling and plaque vulnerability. *Circulation*. 2002;105:939–943.
47. Pasterkamp G, Schoneveld AH, Hijnen DJ, de Kleijn DP, Teepen H, van der Wal AC, Borst C. Atherosclerotic arterial remodeling and the localization of macrophages and matrix metalloproteases 1, 2 and 9 in the human coronary artery. *Atherosclerosis*. 2000;150:245–253.
48. Saam T, Underhill HR, Chu B, Takaya N, Cai J, Polissar NL, Yuan C, Hatsukami TS. Prevalence of American Heart Association type VI carotid atherosclerotic lesions identified by magnetic resonance imaging for different levels of stenosis as measured by duplex ultrasound. *J Am Coll Cardiol*. 2008;51:1014–1021.
49. Takaya N, Yuan C, Chu B, Saam T, Polissar NL, Jarvik GP, Isaac C, McDonough J, Natiello C, Small R, Ferguson MS, Hatsukami TS. Presence of intraplaque hemorrhage stimulates progression of carotid atherosclerotic plaques: a high-resolution magnetic resonance imaging study. *Circulation*. 2005;111:2768–2775.
50. Underhill HR, Yuan C, Yarnykh VL, Chu B, Oikawa M, Polissar NL, Schwartz SM, Jarvik GP, Hatsukami TS. Arterial remodeling in the subclinical carotid artery disease. *J Am Coll Cardiol Cardiovasc Imaging*. 2009;2:1381–1389.
51. Aoki S, Aoki K, Ohsawa S, Nakajima H, Kumagai H, Araki T. Dynamic MR imaging of the carotid wall. *J Magn Reson Imaging*. 1999;9:420–427.
52. Wasserman BA, Casal SG, Astor BC, Aletras AH, Arai AE. Wash-in kinetics for gadolinium-enhanced magnetic resonance imaging of carotid atheroma. *J Magn Reson Imaging*. 2005;21:91–95.
53. Ibrahim T, Makowski MR, Jankauskas A, Maintz D, Karch M, Schachoff S, Manning WJ, Schomig A, Schwaiger M, Botnar RM. Serial contrast-enhanced cardiac magnetic resonance imaging demonstrates regression of

hyperenhancement within the coronary artery wall in patients after acute myocardial infarction. *J Am Coll Cardiol Cardiovasc Imaging*. 2009;2:580–588.
54. Calcagno C, Cornily JC, Hyafil F, Rudd JH, Briley-Saebo KC, Mani V, Goldschlager G, Machac J, Fuster V, Fayad ZA. Detection of neovessels in atherosclerotic plaques of rabbits using dynamic contrast enhanced MRI and 18F-FDG PET. *Arterioscler Thromb Vasc Biol*. 2008;28:1311–1317.
55. Golino P, Ashton JH, Buja LM, Rosolowsky M, Taylor AL, McNatt J, Campbell WB, Willerson JT. Local platelet activation causes vasoconstriction of large epicardial canine coronary arteries in vivo: thromboxane A2 and serotonin are possible mediators *Circulation*. 1989;79:154–166.
56. Willerson JT, Campbell WB, Winniford MD, Schmitz J, Apprill P, Firth BG, Ashton J, Smitherman T, Bush L, Buja LM. Conversion from chronic to acute coronary artery disease: speculation regarding mechanisms. *Am J Cardiol*. 1984;54:1349–1354.
57. Willerson JT, Golino P, Eidt J, Campbell WB, Buja LM. Specific platelet mediators and unstable coronary artery lesions: experimental evidence and potential clinical implications. *Circulation*. 1989;80:198–205.

CLINICAL PERSPECTIVE

Rupture or erosion of vulnerable atherosclerotic plaque is responsible for a substantial number of deaths and disabilities worldwide. Thus, in situ detection of plaques at high risk of disruption and thrombosis may improve risk prediction and treatment of individuals with atherosclerotic disease. The present study describes the use of MRI to identify characteristics of vulnerable plaques in a rabbit model of controlled plaque disruption. Our findings are promising because they are noninvasive, do not entail the use of ionizing radiation or nephrotoxic contrast agents, and can be performed with clinical MRI scanners. Furthermore, the development and testing of drugs to stabilize vulnerable plaques is a major challenge. Because atherosclerosis progression in humans is slow and large patient numbers are required for pharmacological studies, the rabbit model could be used to test the efficacy of therapeutic strategies on plaque morphology. If future investigations find that arterial remodeling and gadolinium uptake have prognostic and clinical value in identifying vulnerable plaques, then the findings of this study can be expanded to monitor the effectiveness of interventions in humans.

SUPPLEMENTAL MATERIAL

In vivo **detection of vulnerable atherosclerotic plaque by magnetic resonance imaging in a rabbit model**

Phinikaridou *et al.*

Supplemental Tables

Table 1: Vessel wall area (mm^2) measured on different MRI images with and without gadolinium

	T1BB	CE-T1BB	CE-PC MRA	*P1*	*P2*	*P3*
Vessel area						
▪ Stable plaque	9.7±2.4	9.5±2.6	8.2±3.2	0.19	0.01	0.01
▪ Vulnerable plaque	12.8±3.0	13.9±4.2	14.6±4.1	0.02	0.02	0.9

P: paired student t-test

P1: T1BB vs. CE-T1BB

P2: T1BB vs. CE-PCMRA (spoiled gradient echo-anatomical images)

P3: CE-T1BB vs. CE-PCMRA

T1BB: T1-weighted black blood images, CE-T1BB: contrast-enhanced (gadolinium) T1-weighted black blood images, CE-PCMRA: contrast-enhanced (gadolinium) phase contrast MRA (T1-weighted spoiled gradient echo images).

Table 2: Frequencies of remodeling types in stable and vulnerable plaque assessed using T1BB, CE-T1BB and CE-PCMRA images

	Stable (n=67)	Vulnerable (n=28)	*P*
Positive remodeling			
▪ T1BB images	37 (55.2)	24 (85.7)	0.009
▪ CE-T1BB	32 (49.2)	23 (76.6)	0.01
▪ CE-PC MRA	15 (22.3)	19 (67.8)	0.01
Negative remodeling			
▪ T1BB images	20 (29.8)	1 (3.7)	0.009
▪ CE-T1BB	12 (17)	3 (10)	0.04
▪ CE-PC MRA	38 (56.7)	4 (14.2)	0.01
Intermediate remodeling			
▪ T1BB images	11 (16.4)	3 (10.7)	0.5
▪ CE-T1BB	21 (32.3)	4 (13.3)	0.05
▪ CE-PC MRA	14 (20.8)	5 (17.8)	0.73

P: x^2 test

T1BB: T1-weighted black blood images

CE-T1BB: contrast-enhanced (gadolinium) T1-weighted black blood images

CE-PCMRA: contrast-enhanced (gadolinium) phase contrast MRA images (T1-weighted spoiled gradient echo images).

Table 3: Comparison of positive remodeling in discriminating stable from vulnerable plaque when calculated using three different types of MRI images

	Sensitivity %	Specificity %	Positive predictive value %	Negative predictive value %	Diagnostic accuracy %
T1BB images	85.7	44.8	88.2	39.3	56.8
CE-T1BB	76.7	50.8	41.8	82.5	58.9
CE-PCMRA	67.8	77.6	55.9	85.2	74.7

T1BB: T1-weighted black blood images

CE-T1BB: contrast-enhanced (gadolinium) T1-weighted black blood images

CE-PCMRA: contrast-enhanced (gadolinium) phase contrast MRA images (T1-weighted spoiled gradient echo images).

Table 4: Plasma lipids and inflammatory markers in rabbits without and with thrombosis

	Rabbits without thrombosis after triggering					Rabbits with thrombosis after triggering						
	Baseline	**8 weeks cholesterol diet**	**4 weeks normal diet**	***P1***	***P2***	**Baseline**	**8 weeks cholesterol diet**	**4 weeks normal diet**	***P1***	***P2***	***P3***	***P4***
Total cholesterol (mg/dL)	172.0±57.0	632±55	596±107.8	0.01	0.01	162±60	654.2±53.4	475.0±177.4	0.01	0.01	0.46	0.17
HDL-cholesterol (mg/dL)	57.5±16.3	37.4±5.9	65.2±13.0	0.03	0.13	63.3±10.7	40.4±8.5	72.0±16.0	0.01	0.11	0.53	0.05
CRP (µg/ml)	2.7±0.5	6.6±5.8	11.2±5.5	0.17	0.01	3.0±0.8	9.6±5.2	13.1±7.6	0.01	0.01	0.35	0.61
PAI-1 (ng/ml)	18.0±4.3	15.7±2.6	17.4±6.4	0.33	0.87	15.7±3.8	17.9±5	20.5±6.7	0.31	0.08	0.39	0.40

P1= baseline vs. 8 weeks cholesterol diet, ***P2***=baseline vs. 4 weeks normal diet, ***P3***=rabbits without thrombosis vs. rabbits with thrombosis at 8 weeks of cholesterol diet, ***P4***=rabbits without thrombosis vs. rabbits with thrombosis at 4 weeks of normal diet.

Table 5: Multiple linear regression analysis of serum biomarkers to indentify predictors of plaque vulnerability

Variables	Odds Ratio	*P* value	95.0% Confidence Interval for Lower Bound	Upper Bound
CRP (baseline)	.858	.156	-1.346	2.586
CRP (8 weeks cholesterol)	.295	.346	-.179	.233
CRP (4 weeks chow)	.973	.090	-.050	.174
PAI-1 (baseline)	-.711	.184	-.424	.246
PAI-1(8 weeks cholesterol)	-.653	.356	-.667	.518
PAI-1 (4 weeks chow)	-.996	.138	-.301	.142
Total cholesterol (baseline)	-.420	.231	-.021	.014
Total cholesterol (8 weeks cholesterol)	-.258	.316	-.019	.014
Total cholesterol (4 weeks chow)	-.467	.157	-.006	.003
HDL-cholesterol (baseline)	.217	.410	-.190	.234
HDL-cholesterol (8 weeks cholesterol)	.351	.446	-.583	.704
HDL-cholesterol (4 weeks chow)	.868	.244	-.437	.650

Supplemental Figures

Figure 1: Receiver operating characteristic curve for the MRI features that discriminate stable and vulnerable plaque

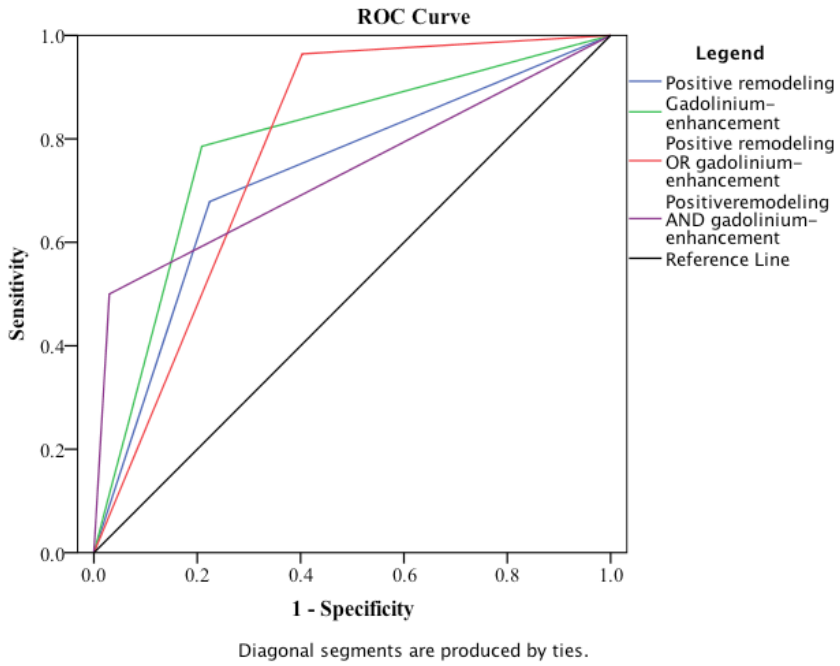

MRI test	Area under the curve
Positive remodeling	0.73
Gadolinium enhancement	0.79
Positive remodeling AND gadolinium-enhancement	0.73
Positive remodeling OR gadolinium-enhancement	0.78

Areas under the curves ranging between 0.7-0.8 indicate a fair diagnostic performance of the MRI features in detecting vulnerable plaque.